Surface Structures of 4-Chlorocatechol Adsorbed on Titanium Dioxide

ARTICLE *in* ENVIRONMENTAL SCIENCE AND TECHNOLOGY · JULY 1996

Impact Factor: 5.33 · DOI: 10.1021/es950872e

5 AUTHORS, INCLUDING:

Michael R. Hoffmann
California Institute of Technology
379 PUBLICATIONS **30,187** CITATIONS

SEE PROFILE

Environ. Sci. Technol. **1996**, *30,* 2535−2542

Surface Structures of 4-Chlorocatechol Adsorbed on Titanium Dioxide

SCOT T. MARTIN, JANET M. KESSELMAN, DAVID S. PARK, NATHAN S. LEWIS, AND MICHAEL R. HOFFMANN*

W. M. Keck Laboratories, California Institute of Technology, Pasadena, California 91125

TiO_2 has been extensively studied as a photocatalyst for the complete oxidation of a variety of organic pollutants commonly found in groundwater. In this paper, we investigate the surface structures formed between an organic substrate and TiO_2 in the context of understanding how these specific surface interactions affect photoreactivity. The surface complexes formed by 4-chlorocatechol (CT) sorbed on TiO_2 are investigated as a function of concentration and of pH. Singular-value decomposition of the IR spectra of CT adsorbed on TiO_2 indicates that a single bidentate chemisorbed species is present over the pH range of 2−10. The surface-bound species appears to have 40% covalent and 60% ionic bond character. The pH dependence of the adsorption isotherms is modeled using a generalized electric double-layer approach. The data are consistent with the formation of a bidentate binuclear surface group for solution CT concentrations below 50 μM followed by nonspecific multilayer partitioning at concentrations above 100 μM.

Introduction

TiO_2 catalyzes the oxidation of chlorinated hydrocarbons in the presence of UV radiation at photon energies equal to or greater than the band-gap energy of 3.2 eV ($\lambda = 385$ nm) (*1*). The quantum efficiency of the process is influenced by electronic processes (*2*−*6*), reactor design (*7*), solution composition (*8*), the organic substrate (*9*), light intensity (*10, 11*), and surface interactions (*12*−*15*). In addition, the interactions between organic ligands and metal oxide surfaces have been the focus of much attention (*16*−*21*). However, the relationship between surface complexation and its effects on TiO_2/UV quantum efficiency has not received as much attention. In this paper, we investigate the surface structures formed between an organic substrate and TiO_2 in the context of understanding how these specific surface interactions affect photoreactivity.

In a previous study, we demonstrated that the trichloroacetate anion is oxidized more quickly at low pH due to electrostatic attraction between the negatively charged anion and the positively charged surface (*10*). On the other hand, the chloroethylammonium cation is oxidized more rapidly as the pH is increased. The interactions between the substrate and surface can be interpreted in part in terms of Gouy−Chapman theory for the activity of the ion at the surface. However, Cunnningham et al. (*12, 13*) found that the rate of photocatalytic oxidation of substituted salicylic acids and monochlorophenols does not correlate with the extent of adsorption. Tunesi et al. (*22*) suggested that salicylate undergoes direct hole transfer at low pH, when it is directly adsorbed to TiO_2, and is attacked by hydroxyl radicals at high pH, when it is found predominantly in solution. Gray (*23*) reported that although the rate of 4-CP loss is independent of catalyst loading, the rate of TOC loss in the same system increases with catalyst loading due to surface-catalyzed thermal reactions. Vasudevan and Stone (*18, 19*) showed that the extent of adsorption of substituted catechols on TiO_2 depends on ionic strength, pH, molecular structure, and the crystalline phase of TiO_2 (i.e., rutile or anatase). Furthermore, the quantum efficiency for the photooxidation of selenite on TiO_2 appears to correlate with the concentration of deprotonated surficial titanol groups (*24*).

In this study using ATR-FTIR spectroscopy, we investigate the surface structures of 4-chlorocatechol (CT) on TiO_2. 4-Chlorocatechol, which adsorbs strongly to metal oxides, is formed as an intermediate in the TiO_2-catalyzed photooxidation of 4-chlorophenol (*8, 25*−*27*). In addition, it is photochemically stable above 340 nm. The C−O stretching frequencies of CT, which shift upon adsorption, occur in an experimentally accessible window of 1000−1500 cm^{-1}.

Experimental Section

Materials. 4-Chlorocatechol (TCI America) is purified by recrystallization from heptane. Titanium dioxide (Degussa P25) is dialyzed against 18 MΩ·cm resistivity water (Millipore) for 4 h to remove 30 μmol/g HCl. This process is repeated three times until the conductivity remains constant. The TiO_2 (1 g/L) is stored up to 6 weeks at 4 °C before use. The BET surface area is 49 m^2/g without thermal activation. All other chemicals are reagent grade.

Acid−Base Titrations. In a 1-L wide-mouth Teflon beaker with screw-top lid, a calomel reference electrode (Beckman) is immersed in electrolyte. A salt bridge (3 wt % agar) connects the reference beaker to the beaker containing the TiO_2 dispersion in order to minimize the effect of the suspension (*28*). In the sample beaker, a pH electrode (Beckman), a bubbler for continuous Ar sparging, and a tube for acid delivery are immersed in 800 mL of 1.25 g/L TiO_2. Both beakers are sealed against the atmosphere and are immersed in a temperature-regulated (25.0 °C) water bath. A typical titration is carried out by adjusting the ionic strength to 1 mM KNO_3 (80.9 mg) and sparging for 60 min with Ar to remove CO_2 and O_2. CT must be handled under anaerobic conditions for pH values above pK_{a1} (8.63) to avoid oxidative coupling (*29*). The pH is adjusted to 10 with NaOH, and 0.1000 N HNO_3 (Baker) is introduced at the rate of 1 mL/h using a syringe pump (Orion Sage Model 361). The syringe pump is calibrated by the mass of titrant added. The pH is continuously monitored using a glass electrode (Beckman) interfaced to

* To whom correspondence should be addressed; telephone 818-395-4391; fax: 818-395-3170; e-mail address: mrh@cco.caltech.edu.

S0013-936X(95)00872-8 CCC: $12.00

Labview for Macintosh (National Instruments). At pH 4, the ionic strength is increased, the pH is returned to 10, and the acid titration is repeated. Blank titrations are carried out in the absence of P25. The H^+ adsorbed on the P25 at any pH is determined by subtracting the moles of H^+ to reach that pH in the absence of P25 from the moles of H^+ necessary to reach that pH in the presence of P25 (*30*). The program FITEQL (*31*) is employed to fit the surface adsorption data to the electric double-layer model to evaluate the total surface concentration of titanol groups and pK_{a1} and pK_{a2} (*32*).

Fluoride Titration. An 800-mL solution containing 1.25 g/L P25 and 10 mM KNO_3 is prepared in a 1-L Teflon beaker (*16*). A combination pH electrode (Beckman), a combination fluoride electrode (Orion 9609B), and an Ar bubbler are immersed in the beaker. The pH is adjusted to 5.5 with HNO_3. The fluoride titration is carried out by adding 80.00 mM NaF at the rate of 233.4 μM/h. The fluoride concentration is continuously monitored with Labview. The F^- adsorbed on TiO_2 is calculated by subtracting the measured solution concentration of fluoride from the total amount of fluoride added to the system.

Batch Adsorption. In a 250-mL three-neck round-bottom flask, 100 mL of 1 g/L TiO_2 and 10 mM KCl are suspended. A combination pH electrode, a 10-mL burette, and 6-in. needles for sampling and Ar sparging enter the sealed flask through rubber septa and stoppers. To carry out a typical adsorption experiment at a fixed pH, 4-chlorocatechol is added as a 1-mL aliquot. After allowing 30 min for equilibration, 500 μL is filtered through 0.45-μm filters. The sample is transferred to a 250-μL reduced volume cuvette and diluted as 10:11 in 1 M HCl. The UV/Vis spectrum is recorded with a HP 8452A diode array spectrophotometer. Both residual TiO_2 and 4-chlorocatechol contribute to the observed spectrum. The components are resolved and quantified by spectral decomposition using Mathematica (Wolfram Research, Champaign, IL). The amount of CT adsorbed to the TiO_2 is calculated by subtracting the measured solution concentration of CT from the total amount of CT added to the solution. To construct the entire adsorption isotherm, further aliquots of CT are added. Samples are taken for analysis on HPLC to confirm the absence of oxidative coupling products according to previously described methods (*25*). Similar adsorption experiments at a fixed concentration of CT and a varying pH are carried out from pH 2 to pH 10. The pH is returned to 2, and a measurement is taken in order to demonstrate the reversibility of adsorption.

FTIR-ATR Measurements. The approach is based upon the methods of Hug and Sulzberger (*21*). (For a general review of reflectance spectroscopy see ref 33.) The ZnSe crystals (trapezoid, 45°, 52.5 mm × 20 mm × 2mm) are freshly coated for each experiment with 2.65 mg of TiO_2 on each side by application of 50 μL of 53 g/L TiO_2. The spectra are recorded using 1024 scans (ca. 40 min) at 8 cm^{-1} resolution on a PE 1600 FTIR spectrophotometer equipped with a Janos F90 ATR optical bench and liquid sample holder. In a typical experiment at a constant pH, the sparged CT solution (10 mM KCl) is flowed through the cell continuously. After at least a 30-min equilibration period, spectra are recorded. The reported spectra are calculated from the subtraction of the spectrum obtained with 10 mM KCl and no CT from the spectrum recorded in the presence of CT. In a typical experiment at a constant [CT] and varying pH, the experiment is carried out by recirculating a 4-L reservoir through the sample cell.

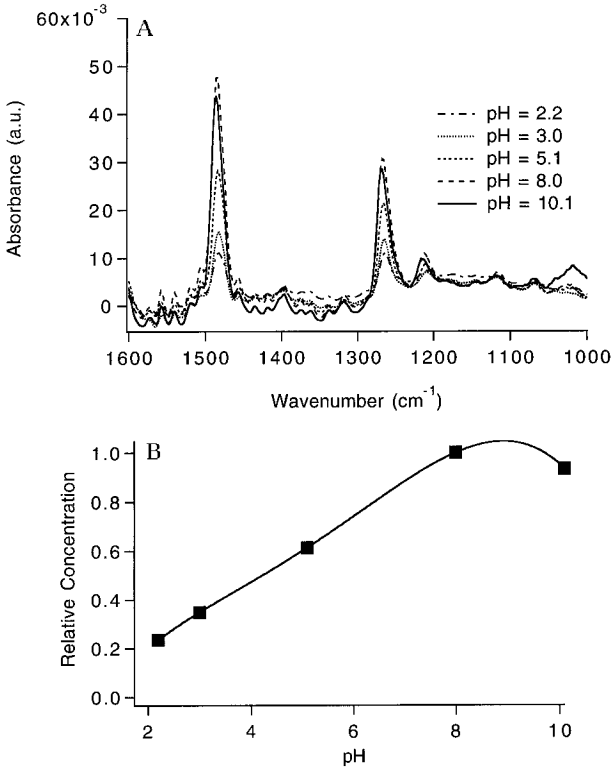

FIGURE 1. (A) IR spectra of 10 μM 4-chlorocatechol adsorbed to TiO_2 at several pHs in 10 mM KCl. Principal component analysis yields one component that explains 96% of the total variance. (B) Relative concentration of adsorbed 4-chlorocatechol as a function of pH (determined by the linear contribution of the first principal component).

FTIR Spectra Calculations. Full details of the computational approach are reported by Hug and Sulzberger (*21*). The elements of the data matrix, $\mathbf{A}_{ij}$, are absorbance values where *i* corresponds to the wavenumber and *j* corresponds to the experimental conditions (e.g., [CT]). Thus, each row contains the absorbance at a fixed wavenumber as a function of changing experimental conditions, and each column contains a spectrum. The **A** matrix may be decomposed by singular-value decomposition as $\mathbf{A} = \mathbf{USV^T}$ where **U** contains the (unrotated) spectral components, **S** contains the singular values, and $\mathbf{V^T}$ contains the loadings. **U**, **S**, and $\mathbf{V^T}$ are reduced according to the number of components implied by S_{ii} (*34, 35*). Furthermore, $\mathbf{A} = \mathbf{BP}$ where **B** contains the physical spectral components (e.g., a surface-adsorbed CT and solution-phase CT), and **P** contains the concentrations of those components as a function of experimental conditions. Before the experiment, **B** is unknown, but the form of $\mathbf{P}_{ij}$ is known. For example, when the first component has the form of a Langmuir isotherm, $\mathbf{P}_{1j} = K[\mathrm{CT}]_j/(1 + K[\mathrm{CT}]_j)$ where $[\mathrm{CT}]_j$ is known and *K* is unknown. There exists some matrix **C** such that $\mathbf{A} = \mathbf{USCC^{-1}V^T}$ so that $\mathbf{B} = \mathbf{USC}$ and $\mathbf{P} = \mathbf{C^{-1}V^T}$. The matrix $\mathbf{C^{-1}}$ rotates $\mathbf{V^T}$ into **P**. We wish to minimize the following objective function:

$$||\mathbf{S}(\mathbf{V^T} - \mathbf{CP})|| \qquad (1)$$

The number of unknowns in the function equals the total number of elements in the **C** matrix plus the *n* unknowns in the **P** matrix (e.g., *K*). To carry out the minimization, we use Mathematica and the simplex method (*36*). If the model

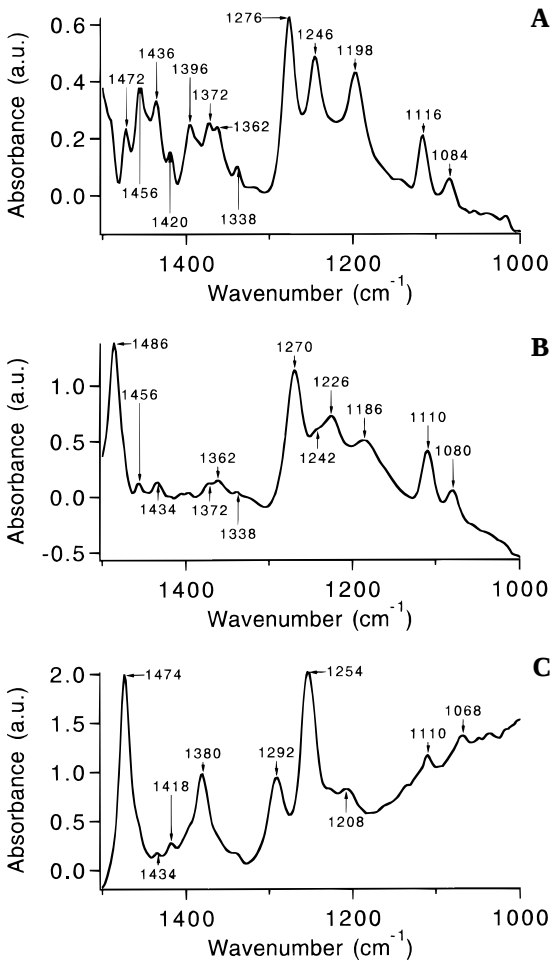

FIGURE 2. IR spectra of 4-chlorocatechol: H_2CT (A), HCT^- (B), CT^{2-} (C). These basis spectra were determined from the singular-value decomposition of 12 spectra recorded at pH 2.72, 5.94, 7.12, 8.02, 8.51, 9.12, 9.6, 11.5, 12.0, 12.6, 13.4, and 13.8.

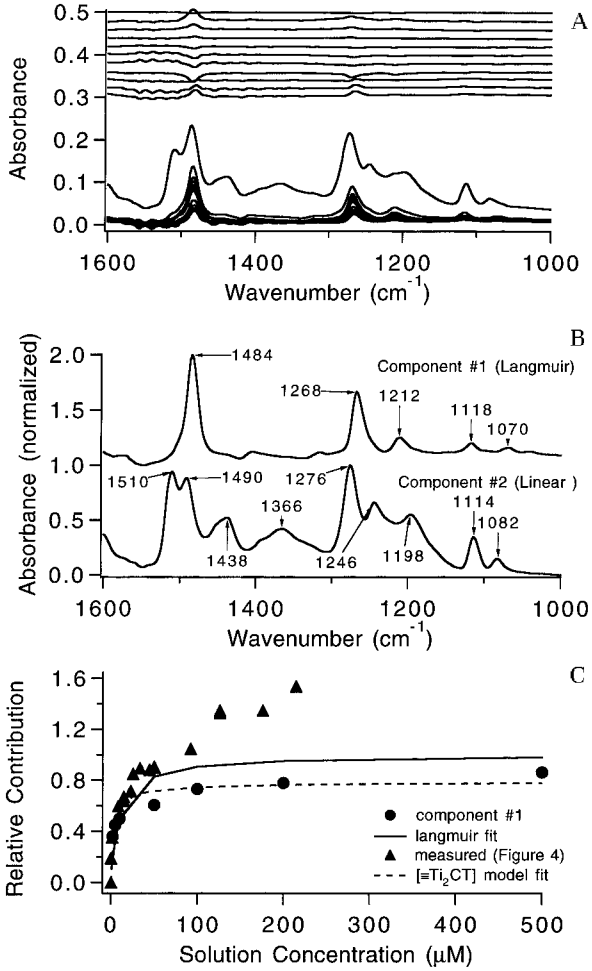

FIGURE 3. (A) IR spectra of 4-chlorocatechol adsorbed on TiO_2 at pH 5.0 in 10 mM KCl at concentrations of 0.002, 0.005, 0.01, 0.05, 0.1, 0.2, 0.5, 1, 2, 10, and 100 mM and the residuals of a fit with a single Langmuirian site ($K = 96\ 577\ M^{-1}$). (B) Component spectra determined from IR data set. (C) Relative concentration of component 1 as compared to measured adsorbed CT (Figure 4).

chosen for the **P** matrix is correct, then **P** and $\mathbf{V}^T$ both span the same subspace and the **C** matrix obtained should yield real components in the **B** matrix. On the other hand, if the model incorporated in the **B** matrix is not correct, a poor minimum is expected and quite possibly negative components in the **B** matrix. Using this technique, we are thus able to decompose the FTIR spectra observed as a function of an experimental condition (e.g., [CT]) into the contributing component spectra and the parameters (e.g., *K*) of the model in the **P** matrix.

Results

Figure 1A shows the IR spectrum of CT adsorbed to TiO_2 as a function of pH. Principal component analysis indicates that one component accounts for 96% of the total variance. The remaining 4% arises from instabilities in the baseline. The sensitivity of detection (ca. 1 μM) has increased significantly because the CT adsorbed to the TiO_2 film is within the penetration depth of the evanescent wave eminating from the ATR crystal. By contrast, the sensitivity toward CT in solution is ca. 10 mM. Figure 1B shows the relative extent of adsorption of CT on TiO_2 as a function of pH. The maximum adsorption is observed at pH 8.

Figure 2 shows the IR spectra of H_2CT, HCT^-, and CT^{2-} in solution as determined from the singular-value decompostion of spectra of CT recorded from pH 2 to pH 14. The total concentration of CT was 40 mM. The minimization of eq 1 yields $pK_{a1} = 8.2$ and $pK_{a2} = 12.7$; the values obtained by Vasudevan and Stone from titration are 8.8 and 12.7, respectively (*19*).

Figure 3A shows IR spectra of CT as a function of concentration (2 μM−100 mM) in contact with a TiO_2 film on the ATR element at pH 5.0 and is qualitatively representative of data recorded from pH 3 to pH 8. The IR spectra are due to contributions from CT adsorbed to TiO_2 and to CT in solution. The spectra are decomposed using a single Langmuir-type binding site on TiO_2 and a linear component in solution. The binding constant obtained from this fitting procedure is 97 000 M^{-1}. Other adsorption models (i.e., Freundlich adsorption or two-site Langmuir models) yield negative peaks in the component spectra. The component spectra determined from the single Langmuir-type binding site are shown in Figure 3B. Residuals (Figure 3A) are calculated by **A** − **BP**. Figure 3C shows the measured contribution of component 1 to the IR spectra and the calculated contribution based on the Langmuir sorption assumption. The Langmuir model underpredicts the observed spectra for 2 and 5 μM while it overpredicts the spectra for 50−500 μM. This error is not accounted for by baseline instabilities and indicates that the Langmuir model does not provide a perfect fit. The model fit obtained from the data in Figure

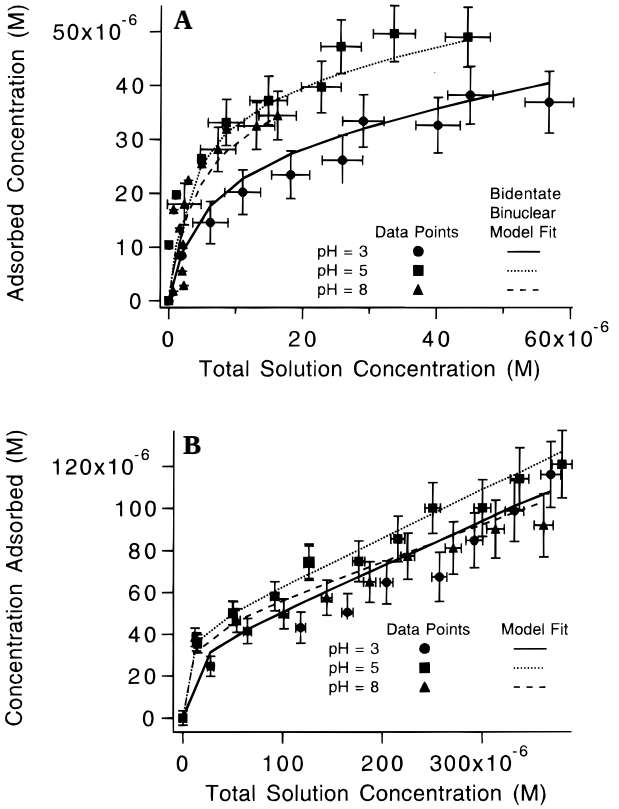

FIGURE 4. Adsorption of 4-chlorocatechol on TiO_2 at pH 3.0, 5.0, and 8.0 as a function of total solution concentration (i.e., $[H_2CT] + [HCT^-] + [CT^{2-}]$). (A) 60 μM maximum concentration. (B) 400 μM maximum concentration. $\sigma_{rel} = 0.02$, $\sigma_{abs} = 2.5$ μM, and $V_y = 0.24$ for model fit (see main text). Some error bars are omitted from the figure for clarity. Conditions: 1 g/L TiO_2, 10 mM KCl, and 25 °C.

4 and the model in Tables 1 and 2 show an improved fit with the FTIR data.

The adsorption isotherms of CT at pH 3, 5, and 8 are shown in Figure 4. At low concentrations (<50 μM), a saturation effect is observed. At high concentrations (>50 μM), linear sorption behavior is observed. The linear region continues to at least 4 mM (data not shown). In the linear region, CT adsorbs to a lesser extent at pH 8 than at pH 3 and 5. The interaction of protons and CT with the surface of TiO_2 is modeled according to the general double-layer theory (*32*). The mass law equations, mole balance equations, and charge−potential relationship used in the model are shown in Table 1. A bidentate binuclear bond between CT and TiO_2 is denoted by $\equiv Ti_2CT$, and a bidentate mononuclear group is shown by $\equiv TiCT[-]$ and carries an overall −1 charge. Different sites of surface groups are denoted by the subscripts A and B. The binding constants of CT at sites A and B are allowed to vary, but the acidity constants for each site are assumed to be the same. The results of considering several surface models constrained by the adsorption isotherms (Figure 4) are shown in Table 2. The best goodness of fit, as indicated by the minimum overall variance (*32*), is obtained for the model including one type of specifically binding bidentate binuclear site on the surface of TiO_2 as well as nonspecific partitioning from the solution to a surface monolayer of CT on TiO_2. The fit obtained with this model is shown in Figures 3 and 4. The linear region observed in the batch adsorption data of Figure 4 is absent in the FTIR data (Figure 3C).

The adsorption isotherms of 49.8 and 498 μM CT on TiO_2 as a function of pH are shown in Figure 5. At both

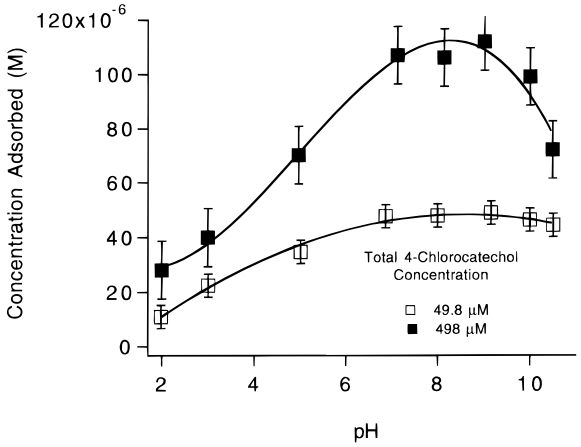

FIGURE 5. Adsorption of 4-chlorocatechol on TiO_2 from pH 2 to pH 11. The total concentration of 4-CC is shown in the legend. Conditions: 1 g/L TiO_2, 10 mM KCl, and 25 °C.

high and low concentrations (i.e., 498 and 49.8 μM), CT is adsorbed most strongly over the range of pH from 7 to 9. At high concentrations, the amount adsorbed varies from 30 to 110 μM from pH 2 to pH 8, whereas at low concentrations it varies from 10 to 45 μM. The sensitivity of adsorption to pH is thus greater at higher [CT]. The fits shown in Figure 5 are an empirical guide and do not arise from an underlying model. In fact, none of the models proposed in Table 2 can adequately reproduce the data shown in Figure 5 under the constraints that the acidity constants $pK_{a1} = 5.8$ and $pK_{a2} = 7.1$, as derived from the data in Figure 6.

The charge due to protons adsorbed on TiO_2 as a function of pH and ionic strength is shown in Figure 6A. The data are fit to the generalized electrical double-layer model. The reactions are shown in Table 1. Model fits are shown (Figure 6A) for optimized values of $[\equiv TiOH] = 75 \pm 5$ μM, $pK_{a1}^{int} = 5.8 \pm 0.4$, and $pK_{a2}^{int} = 7.1 \pm 0.4$. The charge due to adsorbed protons diverges from the model at basic pH for high electrolyte concentrations. The pH_{zpc} obtained from the best fit model is 6.4; other authors have reported for P25 that $pH_{zpc} = 6.6$ (*37*), 6.5 (*18*), and 6.4 (*38*). In Figure 6B, the fluoride adsorption isotherm is shown. The model calculations use the values of pK_{a1}^{int} and pK_{a2}^{int} and optimize for $[\equiv TiOH]$ and $\log K_F-$, which are found to be 35 μM and 10.3 M^{-2}, respectively.

Discussion

The IR spectra of H_2CT, HCT^-, and CT^{2-} in aqueous solution as deduced from SVD analysis of the pH dependent spectra are shown in Figure 2. The bands for H_2CT from 1472 through 1338 cm^{-1} have been assigned to the tangential C−C normal modes of the aromatic rings, and the bands at 1276 and 1246 arise from radial stretching vibrations including the C−O groups, at 1198 from in-plane O−H vibrations, and at 1116 and 1084 from in-plane C−H bending (*39*). Monodeprotonation (Figure 2B) broadens all bands due to the formation of two resonance structures of the hydrogen-bonded bridged species. In addition, all bands are observed to shift to lower energies relative to the neutral form of CT due to the presence of a negative charge that electrostatically destabilizes the molecule and reduces the force constants (*40*). The spectrum of the doubly deprotonated species (Figure 2C) shows a further shift to

TABLE 1

Mass Law and Mole Balance Equations for Model Fits Shown in Table 2, Figure 4, and Figure 6

Components: H^+, $\equiv TiOH_A$, $\equiv TiOH_B$, K^+, NO_3^-, F^-, H_2CT

Species: H^+, OH^-, $\equiv TiOH_A$, $\equiv TiOH_2^+{}_A$, $\equiv TiO_A^-$, $\equiv TiCT^-{}_A$, $\equiv Ti_2CT_A$, $\equiv TiOH_B$, $\equiv TiOH_2^+{}_B$, $\equiv TiO_B^-$, $\equiv TiCT^-{}_B$, $\equiv Ti_2CT_B$, K^+, NO_3^-, F^-, $\equiv TiF_A$, H_2CT, HCT^-, CT^{2-}, CT_{Ads}, CT'_{Ads}

Mass Law Equations

$[H^+]$	=	$[H^+]^1$							
$[OH^-]$	=	$[H^+]^{-1}$	a^{-2}						K_w
$[K^+]$	=						$[K^+]^1$		
$[NO_3^-]$	=		a^{-2}					$[NO_3^-]^1$	
$[H_2CT]$	=					$[H_2CT]^1$			
$[HCT^-]$	=	$[H^+]^{-1}$	a^{-2}			$[H_2CT]^1$			$10^{-8.63}$
$[CT^{2-}]$	=	$[H^+]^{-2}$	a^{-6}			$[H_2CT]^1$			$10^{-21.33}$
$[\equiv TiOH_A]$	=			$[\equiv TiOH_A]^1$					
$[\equiv TiOH_2^+{}_A]$	=	$[H^+]^1$	a^1	$[\equiv TiOH_A]^1$	γ^1				$(1/K_{a1}^{int})$
$[\equiv TiO_A^-]$	=	$[H^+]^{-1}$	a^{-1}	$[\equiv TiOH_A]^1$	γ^{-1}				K_{a2}^{int}
$[\equiv TiCT^-{}_A]$	=	$[H^+]^{-1}$	a^{-1}	$[\equiv TiOH_A]^1$	γ^{-1}	$[H_2CT]^1$			K_A
$[CT_{Ads}]$	=	$[H^+]^{-1}$	a^{-1}	$[\equiv TiOH_A]^1$	γ^{-1}	$[H_2CT]^2$			K_{Ads}
$[\equiv Ti_2CT_A]$	=			$[\equiv TiOH_A]^m$		$[H_2CT]^1$			K_A'
$[CT'_{Ads}]$	=			$[\equiv TiOH_A]^m$		$[H_2CT]^2$			K_{Ads}'
$[\equiv TiOH_B]$	=			$[\equiv TiOH_B]^1$					
$[\equiv TiOH_2^+{}_B]$	=	$[H^+]^1$	a^1	$[\equiv TiOH_B]^1$	γ^1				$(1/K_{a1}^{int})$
$[\equiv TiO_B^-]$	=	$[H^+]^{-1}$	a^{-1}	$[\equiv TiOH_B]^1$	γ^{-1}				K_{a2}^{int}
$[\equiv TiCT^-{}_B]$	=	$[H^+]^{-1}$	a^{-1}	$[\equiv TiOH_B]^1$	γ^{-1}	$[H_2CT]^1$			K_B
$[\equiv Ti_2CT_B]$	=			$[\equiv TiOH_B]^m$		$[H_2CT]^1$			K_B'
$[F^-]$	=							$[F^-]^1$	
$[\equiv TiF_A]$	=	$[H^+]^1$		$[\equiv TiOH_A]^1$				$[F^-]^1$	K_{F^-}

Mole Balance Equations

TOT[H]	=	$[H^+] - [OH^-] - [HCT^-] - 2[CT^{2-}] + [\equiv TiOH_2^+{}_A] - [\equiv TiO_A^-] - [\equiv TiCT^-{}_A] + [\equiv TiOH_2^+{}_B] - [\equiv TiO_B^-] - [\equiv TiCT^-{}_B] + [\equiv TiF_A]$
TOT[a]	=	$0.5\,[H^+] + 0.5\,[OH^-] + 0.5\,[K^+] + 0.5\,[NO_3^-] + 0.5\,[F^-] + 0.5\,[HCT^-] + 2[CT^{2-}]$
TOT[$\equiv TiOH_A$]	=	$[\equiv TiOH_A] + [\equiv TiOH_2^+{}_A] + [\equiv TiO_A^-] + [\equiv TiCT^-{}_A] + 2[\equiv Ti_2CT_A]$
TOT[$\equiv TiOH_B$]	=	$[\equiv TiOH_B] + [\equiv TiOH_2^+{}_B] + [\equiv TiO_B^-] + [\equiv TiCT^-{}_B] + 2[\equiv Ti_2CT_B]$
TOT[K^+]	=	$[K^+]$
TOT[NO_3^-]	=	$[NO_3^-]$
TOT[F^-]	=	$[F^-] + [\equiv TiF_A]$
TOT[H_2CT]	=	$[H_2CT] + [HCT^-] + [CT^{2-}] + [\equiv TiCT^-{}_A] + [\equiv Ti_2CT_A] + [\equiv TiCT^-{}_B] + [\equiv Ti_2CT_B] + [CT_{Ads}] + [CT'_{Ads}]$
TOT[γ]	=	$\equiv TiOH_2^+{}_A] - [\equiv TiO_A^-] - [\equiv TiCT^-{}_A] + [\equiv TiOH_2^+{}_B] - [\equiv TiO_B^-] - [\equiv TiCT^-{}_B] = \sigma(AS/F)$

Charge-Potential Relationship

$$\sigma = 0.1174\, c^{1/2} \sinh(19.46\,\Psi)$$

where σ is the surface charge (C/m^2), c is the ionic strength (M) and equals TOT[a], Ψ is the surface potential (volts), m is assumed to be 1 (16), a is the ionic strength correction term [Fiteql manual], γ is the electrostatic correction term given by $\exp(-F\Psi/RT)$, A is the surface area (m^2/g), S is the oxide loading (g/L), and $\equiv X$ denotes a surface species. Omitted equilibrium constants are unity. See further discussion in text.

lower energies due to electrostatic repulsion. For example, the C−C normal mode shifts from 1490 to 1486 and finally to 1474 while the C−O bond moves from 1276 to 1270 and to 1254 for the neutral, singly deprotonated, and doubly deprotonated species, respectively. The 1198 out-of-plane O−H wag is absent for the doubly deprotonated species.

The IR spectrum of CT adsorbed onto TiO_2 is shown in Figure 3 (B, component 1). We conclude by the similarities between this spectrum and that of the doubly deprotonated CT^{2-} (Figure 2C) that CT forms a bidentate structure on TiO_2. In this case, the band at 1484 arises from C−C normal modes and at 1268 from C−O vibrations. The relative oscillator strengths between these bands and those at 1380 and 1292 in Figure 2 have increased 5-fold. The peaks at 1484 and 1268 in the adsorbed CT spectrum lie between the corresponding peaks for the singly and doubly deprotonated solution phase CT. A linear interpolation based on the peak positions of the solution-phase species as a function of charge suggests that the CT adsorbate carries a charge of −1.2. In a purely covalent bond, we would expect the charge to be 0. This analysis suggests that the bond may be described as having 60% ionic and 40% covalent character. Within experimental error, the peak positions in the IR spectrum of the CT adsorbate do not depend on pH.

The surface adsorbed component is shown in Figure 1A to be qualitatively identical from pH 2 to pH 10, though the extent of adsorption differs (Figure 1B). Furthermore, the line widths are of comparable broadness to those of CT in solution (Figure 2). The heterogeneity of surface energies is thus less than or equal to the distribution of energies found in a solvation shell of water (*40*).

As indicated by the IR spectrum of component 1 in Figure 3, CT forms a bidentate group at the surface of TiO_2. Bidentate mononuclear and binuclear structures are both

TABLE 2

Summary of Agreement Between Proposed Adsorption Models and Experimental Data (Figure 4)[a]

Description	Variance, V_y	$[\equiv TiOH]_A$ (μM)	$[\equiv TiOH]_B$ (μM)	log K_A (-)	log K_B (-)	log K_A' (M^{-1})	log K_B' (M^{-1})	log K_{ads} (M^{-1})	log K_{ads}' (M^{-1})
1 bidentate mononuclear	1.55	264		-1.96					
2 bidentate mononuclear	0.54	751	34.1	-3.46	-0.66				
1 bidentate mononuclear 1 nonspecific binding	1.57	259		-1.93				-0.20	
1 bidentate binuclear	1.25	179				4.38			
1 bidentate binuclear 1 nonspecific binding	0.24	88.5				5.27			8.93
2 bidentate binuclear	1.13	86.0	108			4.65	3.97		
1 bidentate mononuclear 1 bidentate binuclear	1.27	179		-5.17		4.38			

[a] See Table 1 for definitions of symbols. V_y is the overall variance.

possible, as follows:

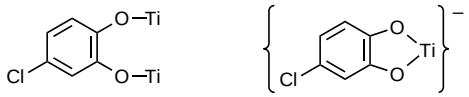

bidentate binuclear $\equiv Ti_2CT$ bidentate mononuclear $\equiv TiCT^-$

The reaction stoichiometries for the formation of $\equiv Ti_2CT$ and $\equiv TiCT^-$ are as follows:

$$2\equiv TiOH + H_2CT \rightarrow \equiv Ti_2CT + 2H_2O \quad (2)$$

$$\equiv TiOH + H_2CT \rightarrow \equiv TiCT^- + H^+ \quad (3)$$

The corresponding mass law equations are shown in Table 1 as K_A' and K_A, respectively. The concentration of the bidentate mononuclear surface group thus has an explicit dependence upon pH; however, both the binuclear and mononuclear surface groups depend implicity upon pH due to the speciation of ≡TiOH, H_2CT, and the surface charge with pH. The pH-dependent adsorption isotherm (Figure 4) should distinguish between the binuclear and mononuclear surface structures.

As shown in Table 2, the adsorption data fit neither a single-site bidentate mononuclear surface structure nor a single-site bidentate binuclear structure. The fit is improved by considering two surface sites, A and B, with different binding affinities for a bidentate mononuclear structure. However, the total concentration of TiO_2 surface sites (785 $\mu M = 8$ sites/nm^2) is much larger than measured for proton affinities (75 μM) or fluoride affinities (35 μM) in Figure 6. The best fit, as indicated by the minimum in V_y and a consistent concentration of surface sites (86 μM), is obtained for a model including a single-site bidentate binuclear surface complex and nonspecific multilayer partitioning from the solution phase according to the following mass law equation:

$$\equiv Ti_2CT + H_2CT \rightarrow CT'_{Ads} \quad (4)$$

The mole balance equation is as follows:

$$H_2CT \rightarrow CT'_{Ads} \quad (5)$$

Incorporated into FITEQL, the mass law equation provides

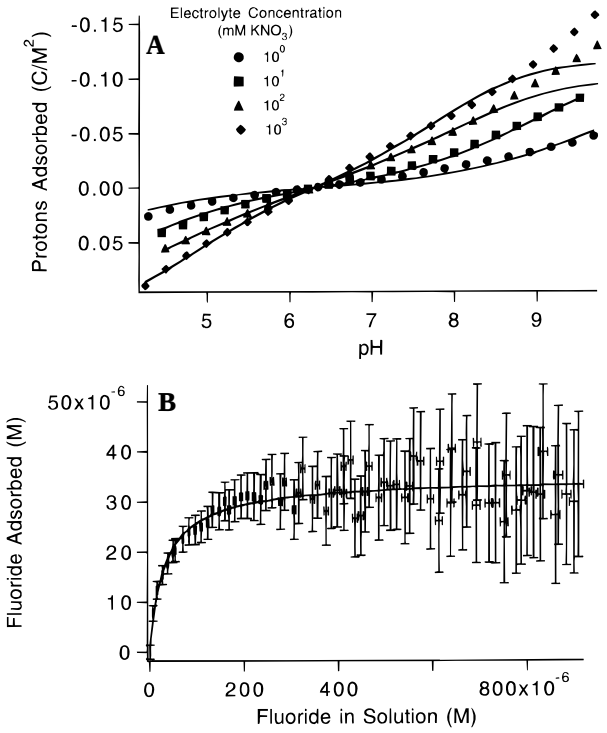

FIGURE 6. (A) Surface charge density due to adsorbed protons as a function of pH and electrolyte concentration as determined by acid titration. Model fits (solid lines) are shown for [≡TiOH] = 75 ± 5 μM, $pK_{a1}^{int} = 5.8 \pm 0.4$, and $pK_{a2}^{int} = 7.1 \pm 0.4$. (B) Adsorbed fluoride concentration as a function of solution concentration of fluoride (pH 5.5 ± 0.2, 10 mM KNO_3). Model fit is shown for [≡TiOH] = 35 μM and log $K_{F^-} = 10.3$ M^{-2}. Conditions: 1.25 g/L TiO_2, Ar sparging, and 25.0 ± 0.1 °C.

increasing affinity for the TiO_2 surface as $[\equiv Ti_2CT]$ increases (i.e., as a monolayer forms) while the mole balance equation indicates the conversion of a solution phase H_2CT to a surface adsorbed species without changing $[\equiv Ti_2CT]_T$ (i.e., nonspecific adsorption).

In order to assess each of the proposed models in Table 2, the appropriate suite of reactions is selected from Table 1. These reactions are constrained by the results of the surface−charge titration (Figure 6A) for which $pK_{a1} = 5.8 \pm 0.4$ and $pK_{a2} = 7.1 \pm 0.4$. The electric double-layer model succeeds in adequately describing the titrations at low ionic strengths, but it underpredicts the surface charge at high ionic strengths and strongly negative surfaces. The TiO_2 employed in the experiments consists of 30-nm primary crystallites agglomerated into 1-μm porous structures (*41*, *42*). The surface charge−potential relationship (i.e., capacitance) in the interstitial pores depends upon the local geometry and should be highly heterogeneous. The double-layer model thus, at best, provides an averaged description of the structure of the TiO_2 since it incorporates Gouy−Chapman theory, which is based upon a flat plane. At low ionic strengths, the Debye-length is several times the size of the primary crystallites and, thus, the pore sizes so that the flat plane description may be adequate. At high ionic strengths, however, the Debye-length compresses and the heterogeneity of the TiO_2 is revealed. Deviation at high ionic strengths from the double-layer theory are thus expected.

As shown in Figure 3C, the specifically adsorbed component observed in the IR spectra approaches saturation above 100 μM. Based upon the the bidentate binuclear model description deduced from the data in Figure 4, we

have calculated the expected concentration of [≡Ti_2CT]. However, because the path length of the ATR cell and the extinction coefficient of the adsorbed species are unknown, a direct comparison between the calculated concentration and the concentration observed in the IR measurements is not possible. Instead, the IR data are calibrated by using the adsorption measurements to provide a best fit of the observed shape. In this case, 1 unit of relative contribution in Figure 3C corresponds to 62 μmol of specifically adsorbed CT/g of TiO_2. Although the ≡Ti_2CT surficial complex is identified by the singular-value decomposition of the IR spectra, the nonspecifically adsorbed CT'_{Ads} is not observed in the FTIR measurements. A nonspecifically associated CT layer should have an IR spectrum similar to the solution-phase molecule. In this case, the basis spectra of two of the three components (i.e., specifically adsorbed, nonspecifically adsorbed, and solution-phase CT) are nearly degenerate so that the SVD procedure reveals only two components. The linear component (Figure 3B, 2) exhibits broadening of the 1438, 1366, 1246, and 1198 cm^{-1} bands relative to the pure solution CT (Figure 2A). The line broadening is consistent both with the heterogeneities in a multilayer environement and two similar components contributing to a single spectrum obtained by SVD.

The IR spectra (Figure 1A) show CT at 10 μM adsorbs to the greatest extent near pH 8 and adsorbs to a lesser extent under more acidic or more alkaline conditions. The IR measurements are supported by the batch adsorption experiments made as a function of pH (Figure 5) at [CT] = 49.8 μM. However, a cross-section of data at [CT] = 50 μM from Figure 4A indicates that the highest concentration of adsorbed CT occurs at pH 5. The reproducibility of the experiments is indicated by the error bars. The apparent inconsistencies between the data sets may be understood by considering the reaction conditions. In the adsorption data of Figure 4, TiO_2 is held at a constant pH for the time course of the experiment (ca. 5 h). In the case of Figures 1 and 5, the TiO_2 is exposed to the highly acidic conditions of pH 2 for 30 min, and the pH is then adjusted upwards. The highly acidic conditions may promote irreversible surface reconstruction. The adsorption behavior of CT on TiO_2 thus depends upon the sample history.

Kummert and Stumm studied the adsorption of catechol on γ-alumina (*17*). Based on the difference in surface charge during titration in the presence and absence of catechols, they conclude that catechol forms a mononuclear monodentate complex on γ-alumina that binds through a single phenolate bridge. However, they also seem to allow for a mononuclear bidentate structure analogous to solution complexes. A bidentate binuclear structure is excluded based on titration data as well as the distance between adjacent hydroxo groups on γ-alumina. McBride and Wesselink studied the adsorption of catechol on a variety of alumina surfaces using FTIR (*43*). The IR spectrum of catechol adsorbed on amorphous alumina is similar to the spectrum we observed for CT on TiO_2. McBride and Wesselink postulate a bidentate structure based on the IR data as well as the much stronger adsorption seen for compounds with ortho functional groups. In contrast to the OH groups on γ-alumina, those of amorphous alumina are close enough to accommodate bidentate binuclear complexes.

Vasudevan and Stone (*19*) studied the adsorption of a variety of catechols including CT on TiO_2, and their data agree with those shown in Figure 5. Using the contraints of $pK_{a1} = 3.9$, $pK_{a2} = 8.7$, and 3−4 sites/nm^2, these authors conclude that CT binds to TiO_2 as negatively charged surface complex as follows:

$$>S + CT \rightarrow [>S{-}CT]^- + H^+ \qquad (6)$$

where >S denotes a neutral TiO_2 surface group. Note the difference in pH dependence between this model and our proposed model of adsorption as given by eq 2. As previously discussed, the pH dependence observed in Figures 4 and 5 differs due to exposure of the TiO_2 particles to extreme pH conditions in the case of Figure 5. The data in Figure 4 were used to model the pH dependence of CT adsorption in our experiments. The added information provided by FTIR data support our hypothesis of a bidentate, binuclear complex.

Unlike Hug and Sulzberger (*21*), who were able to distinguish multiple binding modes for sulfate and oxalate on TiO_2, we observe only one specific binding mode for adsorbed catechol in our experiments. The additional information provided by the titration and batch adsorption experiments and the resulting modeling studies lend confidence to our hypothesis of one specifically adsorbed surface species.

In conclusion, 4-chlorocatechol adsorbs as a bidentate binuclear surface complex on TiO_2 at solution concentrations below 50 μM. Above that concentration, CT adsorbs nonspecifically in a multilayer environment. The specifically adsorbed CT appears to have 40% covalent and 60% ionic bond character. In ongoing work, we will study the photoreactivity of CT in the TiO_2/UV process. Based upon this work, when [CT] = 50 μM, maximum quantum efficiencies are expected to occur at pH = 5. When [CT] = 500 μM, catalyst poisoning may occur due to charge−carrier recombination if an electron acceptor is unable to penetrate the CT multilayer.

Acknowledgments

We are grateful to ARPA and ONR (NAV 5 HFMN N0001492J1901) for financial support. Drs. Ira Skurnick and Harold Guard provided generous support and encouragement. S.T.M. is supported by a National Defense Science and Engineering Graduate Fellowship. J.M.K. is the recepient of a National Science Foundation Predoctoral Fellowship. D.S.P. is a Summer Undergraduate Research Fellow. Wonyong Choi, Peter Green, and Nicole Peill provided critical analyses and stimulating discussion.

Literature Cited

(1) Hoffmann, M. R.; Martin, S. T.; Choi, W.; Bahnemann, D. W. *Chem. Rev.* **1995**, *95*, 69.
(2) Martin, S. T.; Herrmann, H.; Choi, W.; Hoffmann, M. R. *J. Chem. Soc. Faraday Trans.* **1994**, *90*, 3315.
(3) Martin, S. T.; Herrmann, H.; Hoffmann, M. R. *J. Chem. Soc. Faraday Trans.* **1994**, *90*, 3323.
(4) Kesselman, J. M.; Shreve, G. A.; Hoffmann, M. R.; Lewis, N. S. *J. Phys. Chem.* **1994**, *98*, 13385.
(5) Herrmann, H.; Martin, S. T.; Hoffmann, M. R. *J. Phys. Chem.* **1995**, *99*, 16641.
(6) Choi, W.; Termin, A.; Hoffmann, M. R. *J. Phys. Chem.* **1994**, *98*, 13669.
(7) Peill, N. J.; Hoffmann, M. R. *Environ. Sci. Technol.* **1995**, *29*, 2974.
(8) Martin, S. T.; Lee, A. T.; Hoffmann, M. R. *Environ. Sci. Technol.* **1995**, *29*, 2567.
(9) Carraway, E. R.; Hoffman, A. J.; Hoffmann, M. R. *Environ. Sci. Technol.* **1994**, *28*, 786.
(10) Kormann, C.; Bahnemann, D. W.; Hoffmann, M. R. *Environ. Sci. Technol.* **1991**, *25*, 494.

(11) Hoffman, A. J.; Carraway, E. R.; Hoffmann, M. R. *Environ. Sci. Technol.* **1994**, *28*, 776.
(12) Cunningham, J.; Sedlák, P. *J. Photochem. Photobiol. A: Chem.* **1994**, *77*, 255.
(13) Cunningham, J.; Al-Sayyed, G. *J. Chem. Soc. Faraday Trans.* **1990**, *86*, 3935.
(14) Stafford, U.; Gray, K.; Kamat, P.; Varma, A. *Chem. Phys. Lett.* **1993**, *205*, 55.
(15) Moser, J.; Punchihewa, S.; Infelta, P. P.; Grätzel, M. *Langmuir* **1991**, *7*, 3012.
(16) Sigg, L.; Stumm, W. *Colloids Surf.* **1981**, *2*, 101.
(17) Kummert, R.; Stumm, W. *J. Colloid Interface Sci.* **1980**, *75*, 373.
(18) Stone, A. T.; Torrents, A.; Smolen, J.; Vasudevan, D.; Hadley, J. *Environ. Sci. Technol.* **1993**, *27*, 895.
(19) Vasudevan, D.; Stone, A. T. *Environ. Sci. Technol.* **1996**, *30*, 1604.
(20) Biber, M. V.; Stumm, W. *Environ. Sci. Technol.* **1994**, *28*, 763.
(21) Hug, S. J.; Sulzberger, B. *Langmuir* **1994**, *10*, 3587.
(22) Tunesi, S.; Anderson, M. *J. Phys. Chem.* **1991**, *95*, 3399.
(23) Gray, K. Personal communication, 1995.
(24) Gruebel, K.; Davis, J.; Leckie, J. *Environ. Sci. Technol.* **1995**, *29*, 586.
(25) Martin, S. T.; Morrison, C. L.; Hoffmann, M. R. *J. Phys. Chem.* **1994**, *98*, 13695.
(26) Mills, A.; Morris, S. *J. Photochem. Photobiol. A: Chem* **1993**, *71*, 285.
(27) Mills, A.; Davies, R. H.; Worsley, D. *Chem. Soc. Rev.* **1993**, *22*, 417.
(28) Bates, R. G. *Determination of pH: Theory and Practice,* 2nd ed.; John Wiley & Sons: New York, 1973.
(29) Taylor, W.; Battersby, A. *Oxidative Coupling of Phenols*; Marcel Dekker: New York, 1967.
(30) Yates, D. E. The Structure of the Oxide/Aqueous Electrolyte Interface. Thesis, University of Melbourne, 1975.
(31) Herbelin, A.; Westall, J. C. *FITEQL 3.1*; Report 94-01; Department of Chemistry, Oregon State Univeristy, 1994.
(32) Dzombak, D.; Morel, F. *Surface Complexation Modeling: Hydrous Ferric Oxide*; John Wiley & Sons: New York, 1990.
(33) Wendlandt, W.; Hecht, H. *Reflectance Spectroscopy*; John Wiley & Sons: New York, 1966.
(34) Pullin, M.; Cabaniss, S. *Environ. Sci. Technol.* **1995**, *29*, 1460.
(35) Shrager, R. I.; Hendler, R. W. *Anal. Chem.* **1982**, *54*, 1147.
(36) Carley, A. F.; Morgan, P. H. *Computational Methods in the Chemical Sciences*; John Wiley & Sons: New York, 1989.
(37) Herrmann, V. M.; Boehm, H. P. *Z. Anorg. Allg. Chem.* **1969**, *368*, 73.
(38) Schindler, P. W.; Gamsjäger, H. *Kolloid Z. Z. Polym.* **1972**, *250*, 759.
(39) Varsanyi, G. *Assignments for Vibrational Spectra of Seven Hundred Benzene Derivatives*; John Wiley & Sons: New York, 1974.
(40) Urban, M. W. *Vibrational Spectroscopy of Molecules and Macromolecules on Surfaces*; John Wiley & Sons: New York, 1993.
(41) Degussa Technical Bulletin No. 56, 1990.
(42) Bickley, R. I.; Gonzalez-Carreno, T.; Lees, J. S.; Palmisano, L.; Tilley, R. J. D. *J. Solid State Chem.* **1991**, *92*, 178.
(43) McBride, M. B.; Wesselink, L. G. *Environ. Sci. Technol.* **1988**, *22*, 703.

Received for review November 21, 1995. Revised manuscript received April 10, 1996. Accepted April 12, 1996.[⊗]

ES950872E

[⊗] Abstract published in *Advance ACS Abstracts,* June 15, 1996.